WILLIAM & MARY
CHARTERED 1693

W&M ScholarWorks

Dissertations, Theses, and Masters Projects

Theses, Dissertations, & Master Projects

1965

Thick Target Bremsstrahlung Production in Silicon

Maurice C. McGee
College of William & Mary - Arts & Sciences

Follow this and additional works at: https://scholarworks.wm.edu/etd

Part of the Physics Commons

Recommended Citation

THICK TARGET BREMSSTRAHLUNG PRODUCTION IN SILICON

A Thesis

Presented to

The Faculty of the Department of Physics

The College of William and Mary in Virginia

In Partial Fulfillment

of the Requirements for the Degree of

Master of Arts

By

Maurice C. McGee

August 1965

THICK TARGET BREMSSTRAHLUNG PRODUCTION IN SILICON

———————

A Thesis

Presented to

The Faculty of the Department of Physics

The College of William and Mary in Virginia

———————

In Partial Fulfillment

Of the Requirements for the Degree of

Master of Arts

———————

By

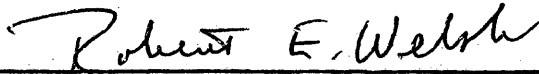Maurice C. McGee

August 1965

APPROVAL SHEET

This thesis is submitted in partial fulfillment of

the requirements for the degree of

Master of Arts

_____
Author

Approved, August 1965

_____
Herbert Funsten, Ph.D.

_____
Robert E. Welsh, Ph.D

_____
Morton Eckhause, Ph.D

ACKNOWLEDGMENTS

TABLE OF CONTENTS

LIST OF FIGURES AND TABLES

ABSTRACT

Angular distributions of bremsstrahlung created by bombarding thick silicon targets with 1.05 Mev and 1.25 Mev electrons have been calculated by measuring the spectra at 10 angles between 0° and 180°. The observed spectra, after appropriate corrections, have been compared with the predictions of the Bethe-Heitler theory. Analytical expressions for the angular distribution of the spectra and total radiated energy are given. Also the experimental and the theoretical efficiencies of the bremsstrahlung production are given for each incident electron energy.

THICK TARGET BREMSSTRAHLUNG PRODUCTION IN SILICON

INTRODUCTION

Since there are electrons trapped in the magnetic field of the earth an evaluation of the radiation hazard to space travelers due to their presence is essential. These electrons can dissipate a sizable part of their energies through radiative collisions in materials. The bremsstrahlung or "Braking Radiation" due to these collisions poses a hazard because of their high penetrating power.

There are adequate theories available for estimates of the bremsstrahlung from thin targets where a thin target is defined as one in which the electron scattering and energy loss processes have a negligible influence on the energy and angular distribution of the bremsstrahlung. These theoretical treatments have been summarized by Koch and Motz (ref. 1).

In the case of bremsstrahlung from a thick target, where a thick target is defined as one which completely stops the electrons, there is no adequate theoretical approach available. This is due mainly to the fact that it is a very complicated procedure which must take into account the multiple scattering of the electron in the target, the fluctuations in the rate of energy loss, and the attenuation of the bremsstrahlung in the target.

It was decided to initiate this program to investigate the bremsstrahlung spectra produced when electrons of 1.05 and 1.25 Mev

strike a thick silicon target. The experimental results are compared with a theoretical model which attempts to account for the thick target complications. Also, the efficiency of the thick target bremsstrahlung production is compared with the theoretically expected values.

CHAPTER I

APPARATUS

The bremsstrahlung was produced when a well collimated electron beam struck a thick silicon target. The target was located inside a chamber where a pressure of the order of 10^{-6} torr was maintained. A schematic diagram of the apparatus is shown in figure 1.

Beam tube assembly.— The first section of the beam tube was a tee fitting which connected the beam tube to the Dynamitron electron accelerator and also provided a connection for an oil diffusion pump. A safety valve was placed after the tee. This safety valve could be pneumatically closed by a switch in the control room in order to protect the electron accelerator in case a vacuum leak developed in the beam tube.

The next section was a collimator used to reduce the electron beam to the desired size and to insure that the electron beam did not drift off the target and hit the chamber wall. The collimator consisted of a 36-inch long piece of rectangular aluminum pipe with two removable sides. Inside the collimator were three sets of · collimating blocks 6 inches apart. Each set consisted of four adjustable carbon blocks. These collimating blocks could be adjusted to form a rectangular opening of desired size to collimate

the electron beam. The temperature of the collimating blocks was monitored with thermocouple temperature gauges to avoid overheating.

The next section was an extension tube which permitted the length of the beam tube to be varied. The length could be increased, for instance, in order to reduce the background from the accelerator. This section was followed by another tee fitting which provided connections for a second diffusion pump and vacuum gauges. The two diffusion pumps were able to evacuate the entire beam tube to a pressure of approximately 10^{-6} torr.

The last section consisted of the target chamber and the angular distribution table. Two different chambers were used during these measurements. Both target chambers were 8 inches in diameter and 4 inches high with a quartz top for viewing. The brass target chamber was connected to the beam tube by a 12-inch long pipe which was 2 inches in diameter. A bleed-off valve that allowed the target chamber to be brought up to atmospheric pressure without opening up the rest of the beam tube was provided. One of the chambers had an exit port opposite the entry port. Attached to this exit port was a 12-inch long aluminum pipe which was closed off at the free end. This aluminum tailpipe allowed the background measurements to be made without disturbing the detection setup. This chamber was used for measurements at angles over 45° with respect to the beam tube. The other chamber, which was used for measurements at angles between 0° and 45° with respect to the beam tube, did not have an exit port opposite the entry port and thus

the background measurements were made by letting the electron beam
strike the back of the target chamber. A tailpipe was not used in
this case because it physically blocked the detector and its
shielding at small angles.

The target holder was mounted through the quartz top by means
of a dynamic O-ring seal. This permitted the target to be rotated,
or raised, or lowered without breaking the vacuum seal.

The table on which the target chambers were mounted was
36 inches in diameter and had four legs of adjustable height to
insure that the plane of incidence containing the electron beam
was normal to the target. An arm 6 inches wide and 20 inches long
was connected to the center of the angular distribution table so
that it would rotate about the center of the target chamber.

Detection system.— The detector for the bremsstrahlung was
a 2-inch by 2-inch NaI (Tl) crystal mounted on a Dumont 6292
photomultiplier tube. This detector was mounted on the arm, which
rotates about the target chamber, at a distance of 12.16 inches
from the center of the target. The detector was shielded from
stray radiation from the sides by lead bricks stacked around it.
The only radiation the detector could receive was through an
8-inch long lead collimator mounted between the detector and the
chamber wall. The collimator had a tapered axial clearance
leading to the center of the target. The collimator hole was
0.925-inch in diameter at the face in contact with the crystal.
The output of this detector after suitable amplification was fed
into a TMC (model No. 402) 400 channel pulse height analyser.
The data were printed out on an IBM typewriter.

In order to correct for possible target deterioration the entire series of measurements were monitored by another 2-inch by 2-inch NaI (Tl) crystal on a Dumont 6292 photomultiplier. This detector was placed 11.0 inches from the target at an angle of 52° from the centerline of the beam tube. The monitor counter output was fed into a single channel analyser (Hamner (moder N 302)). The discriminator on the single channel analyzer was set to accept all pulses above 500 kev. The output of the analyzer was counted on a scaler.

Beam integration.— In order to determine the total number of electrons incident on the target during each run, Elcor current integrators (model No. 309B) were attached to both the target and the target chamber. The target holder was insulated from the target chamber and the target chamber was insulated from the beam tube. The current integrator made it possible to determine the total number of electrons striking the target during an experimental run and to determine the total number of electrons striking the target chamber during a background run. The current integrators were also used to focus the electron beam on the target. This is done by focusing until the maximum amount of current is read on the target and the minimum amount of current is read on the target chamber.

Target preparation.— In this experiment thick silicon targets were used. A target is defined as thick if its thickness equals the range of the appropriate electrons. For the 1.25 Mev electrons the samples were 2.28 mm thick and for the 1.05 Mev electrons the samples were 1.88 mm thick.

The electron range was calculated using the Katz and Penfold (ref. 4) empirical relation.

$$R \text{ mg/cm}^2 = 4.12 \, E^n$$

where

$$E = \text{electron energy in Mev}$$
$$n = 1.265 - 0.0954 \, \log_e E$$

The ranges computed from this formula were increased by 10 percent to take the electron straggling into effect.

The chemically pure silicon, obtained from the Eagle-Picher Company, was cut into targets one square centimeter in area and of the appropriate thickness, after which they were ultrasonically cleaned.

CHAPTER II

EXPERIMENTAL PROCEDURE

With the apparatus set up as described in chapter I, electron beams of the order of 2×10^{-9} amperes and of energy 1.05 Mev from a dynamitron electron accelerator were focused on the thick silicon target. The energy determinations are based on range-energy relationships for electrons in aluminum and consequently are accurate to about 5 percent. A Ling television camera in conjunction with a zinc sulfide screen was used to help focus the beam on the target. The television camera and zinc sulfide screen were used to roughly focus the electron beam on target and the electrometers described in chapter I were used to accurately focus the electron beam on the target. The carbon collimators prevented the beam from shifting from the target to the chamber wall due to a change in the current of the focussing coils. However, the bremsstrahlung from the collimators did not interfere with the experiment since the detector was well shielded except from the target.

The bremsstrahlung spectra at various angles were recorded in the memory of the multichannel analyzer. The time for each run was determined by a preset number of counts on the fixed detector. The measurements were made at the angles of 5°, 15°, 30°, 45°,

9

60°, 75°, 90°, 105°, 120°, and 130° with respect to the beam tube. During each run the beam current hitting the target and the target chamber was monitored. Also, a background measurement was made at each angle. For angles greater than 45° the target was pulled out of the beam and the spectrum produced by the electrons striking the end of the long aluminum pipe was measured. For angles less than 45° the background measurement was made by pulling the target out of the beam and letting the electrons strike the back of the target chamber. The total current striking the chamber was also recorded.. In addition to these measurements a calibration spectrum of the pulse height analyzer using a Co^{60} and Cs^{137} source was made every 10th run.

This entire process was repeated for the incident electron energy of 1.25 Mev.

CHAPTER III

EXPERIMENTAL RESULTS

The observed bremsstrahlung spectra for 1.05 and 1.25 Mev electrons at 45° and 105° are shown in figures 2, 3, 4, and 5, respectively. These spectra are typical of the bremsstrahlung data taken in this experiment. In order to be of use several corrections had to be applied to these spectra.

It was necessary to correct for the finite resolution of the sodium iodide crystal for photons of different energies. The experimental spectra were divided into "energy strips" and each 50 kev wide. A representative pulse "profile" of each "strip" was obtained from the Cs^{137} and Co^{60} calibration spectra, (fig. 6). Starting with the highest "energy strip," a representative pulse due to a γ-ray of energy equal to the energy at the middle of the "strip" was drawn in. The total capture peak of this representative pulse was located at the mid-point of the strip and its height matched the mid-strip intensity. This pulse was subtracted from the entire spectrum and the next "strip" was then treated in the same manner. This process was continued until the last "strip" was reached. The area under each of the pulses was then calculated. This area is proportional to the number of X-rays in the energy range determined by the "energy strip" boundaries. In this manner,

11

the true observed counts in 50 kev energy intervals were obtained. These counts were then corrected for the counting rate effect. This effect is due to the fact that the analyzer has a "dead time." This correction is made by multiplying the counts in each "strip" by the ratio.

$$\left[\frac{\text{clock time}}{\text{live time}}\right]$$

The spectrum at each angle was treated in this manner.

When the electrons strike the target some of them are back-scattered and strike the chamber wall producing bremsstrahlung. In order to determine these background spectra, experimental runs were made by pulling the target out of the beam and letting the electrons strike the back of the target chamber for a predetermined time. The background bremsstrahlung spectra were then analyzed in the same manner as the main spectra to correct for the effects of the finite resolution of the detector. Then "normalization" corrections were applied to correct for:

(1) the position of the bremsstrahlung production,

(2) the amount of charge producting the background bremsstrahlung, and

(3) the atomic number of the material producing the background bremsstrahlung.

Because bremsstrahlung intensity is inversely proportional to the square of the distance from the source, directly proportional to the number of electrons producing the bremsstrahlung, and directly proportional to the square

of the atomic number of the material producing the bremsstrahlung, and since the detector was equally shielded from all sides except the target, we used the following normalization factor.

$$C_2 = C_1 \left[\left(\frac{d_1}{d_2}\right)^2 \left(\frac{Q_2}{Q_1}\right) \left(\frac{Z_2}{Z_1}\right)^2 \right]$$

where C_2 = normalized background counting rate

C_1 = unnormalized background counting rate

d_2 = average distance from the detector to the points where the scattered electrons struck the chamber wall

d_1 = distance from the detector to the point where electron beam of the background measurement struck the target chamber or aluminum tailpipe

Q_2 = the charge collected by the chamber when the beam was incident on the target

Q_1 = the total charge striking the chamber or aluminum pipe during background run

Z_2 = the average atomic number of brass given by:

$$Z_{eff} = \frac{N_{cu} Z_{cu} + N_{zn} Z_{zn}}{N_{cu} + N_{zn}} = 31$$

Z_1 = atomic number of material struck by electron beam during background measurement

After the background had been normalized it was then corrected for the counting rate effect.

At this point the background spectra were subtracted from their respective target spectra. In figures 2, 3, 4, and 5 it is seen that the background is small compared to the target spectra. The resulting spectra were then corrected for the absorption of the bremsstrahlung in the chamber wall and in the aluminum cover over the sodium iodide crystal, and for the efficiency of the detector which is shown in figure 7. The expression for this is,

$$N_{true} = \frac{N_{corrected} \; e^{u_1 x_1 + u_2 x_2}}{detector \; effeciency}$$

$N_{corrected}$ = number of counts in spectra corrected for resolution of detector, counting rate effect, and background.

N_{true} = number of counts in a completely corrected spectra.

where u_1 = absorption coefficient of brass

x_1 = thickness of chamber wall

u_2 = absorption coefficient of aluminum

x_2 = thickness of aluminum shield over crystal

The spectra then represented the true bremsstrahlung at each angle. The spectra at 45° and 105° for both incident electron energies were then compared with the theoretical results. These spectra are shown in figures 8, 9, 10, and 11.

The spectra at all angles were divided into three sections. For the 1.25 Mev electrons the sections included X-rays from 1250 kev to 850 kev, from 850 kev to 450 kev, and from 450 kev to 100 kev. For the 1.05 Mev electrons the sections included X-rays from 1050 kev to 750 kev, from 750 kev to 450 kev, and from 450 kev to 150 kev.

The total number of counts in each of these sections was added together. Plots of the angular distribution of the total counts in the sections are shown in figures 12 and 13. Using least square analysis the distribution of these sections were fitted to an analytical expression of the form.

$$w(\theta) = A_0 + A_1 \, P_1 \, (\cos \, \theta) + A_2 \, P_2 \, (\cos \, \theta) + \cdot \cdot \cdot$$

where $w(\theta)$ = angular distribution function

   A_i = coefficient of Legendre polynomial of the ith order

These expressions are shown in table I.

The total intensity at each angle, defined as the sum of the counts multiplied by their respective energy, is obtained by multiplying the mean energy of each 50 kev strip by the true number of counts in the strip. Then the total intensity of the strips at each angle is obtained. The total intensity at each angle is then normalized for a standard number of incident electrons. Plots of the angular distribution of total intensity are shown in figures 14 and 15. Again, a least-squares analyses was applied to obtain an analytical expression for the distribution of the total intensity. These expressions are shown in table II.

The expressions for the angular distribution of the total intensity at incident electron energies of 1.05 and 1.25 Mev were then integrated over all angles θ and ϕ in order to obtain the total radiated energy. The expression used was

$$I = \int I(\theta)d\Omega = 2\pi \int_0^\pi I(\theta)\sin\theta\,d\theta$$

From the total radiated energy and the total incident electron energy the efficiencies of the radiative collisions were calculated. That is,

$$\epsilon = \frac{\text{total radiated energy}}{\text{total incident electron energy}}$$

The results thus obtained were compared with theoretical values as shown in table III.

CHAPTER IV

THEORY

When an energetic electron strikes a target there are four
principal types of interaction by which it may lose its energy or
be scattered. It could undergo elastic scattering with the atomic
electrons or with the nucleus. Elastic scattering in the field
of the atomic electrons is really an interaction with the atom as
a whole. However, such collisions are only significant for very
low energy electrons. On the other hand there is a high probability
that the electron will undergo nuclear elastic scattering. Here
the only kinetic energy lost is that necessary for the conservation
of momentum.

The incident electron could also undergo inelastic collisions
with the atomic electrons or the nucleus. The inelastic collisions
with the atomic electrons, resulting in the ionization or the
excitation of the atom, are usually the most predominant interactions
by which an incident electron would lose energy. There is a very
small probability that the nucleus will undergo coulomb excitation
by an incident electron; however, there is a greater probability for
inelastic electron scattering in the field of the nucleus due to
the fact that every time an electron is deflected by a nucleus there
is a finite probability that a quantum of radiation will be emitted.

This radiation is called **bremsstrahlung** and, the energy of the bremsstrahlung corresponds to the kinetic energy lost by the incident electron.

In the case of an electron incident on a thick target, the electron will suffer a number of collisions with nuclei, in each of which it will experience an acceleration deflecting it from its original path. The classical explanation of bremsstrahlung predicts that every time an electron is accelerated it should emit electromagnetic radiation. A classical treatment gives the result that the differential radiation probability is dependent on the square of the atomic number of the target material and is inversely dependent on the square of the mass of the incident particle. However the dependence on Z^2 was found to hold only for thin target bremsstrahlung. Thick target bremsstrahlung is approximately dependent on the first power of Z. This is due to the fact that at electron energies of a few Mev and below, the range of an electron is controlled almost entirely by ionizing collisions with the orbital electrons of the target material. Therefore, the number of nuclei encountered by the electron before it is completely stopped is roughly proportional to $\frac{1}{Z}$. Therefore the Z^2 is reduced to Z.

However, the quantum mechanical treatment of bremsstrahlung describes the event in terms of a certain probability of the electron's making a transition from one state to another with the emission of a photon. Therefore, as was stated at first, when an electron is scattered by a nucleus the highest probability is for an elastic collision; but there is a chance of a radiative collision.

The cross section for the radiative collisions is of the order of $\frac{1}{137}$ times the cross section for elastic scattering.

Although the classical theory predicts a small amount of energy radiated with every deflection and the quantum theory predicts a small number of larger energy losses, the averages are about the same for the two theories.

The theoretical analysis of thick target bremsstrahlung is however a complicated procedure. The amount of energy loss and the deflection of the electron as it passes through the material, and the absorption of the X-rays inside the material must all be included in calculations. These effects, with some simplifications, have been included in the calculation of the theoretical bremsstrahlung spectra using the Bethe and Heitler theory (ref. 2).* The simplifications introduced in the theoretical calculations have not reduced the rigor of the treatment appreciable.

The thick foil was treated as if it were made up of a large number of thin foils, each of which produced the same energy loss through ionization and excitation.

Multiple scattering effects in each foil were evaluated using the Goudsmidt-Sanderson theory. The absorption effects of the target were approximately allowed for by assuming that, on the average, each photon will have to travel through half the thickness of the target.

---

*The theoretical calculations were obtained from Dr. J. J. Singh and are given in reference 2.

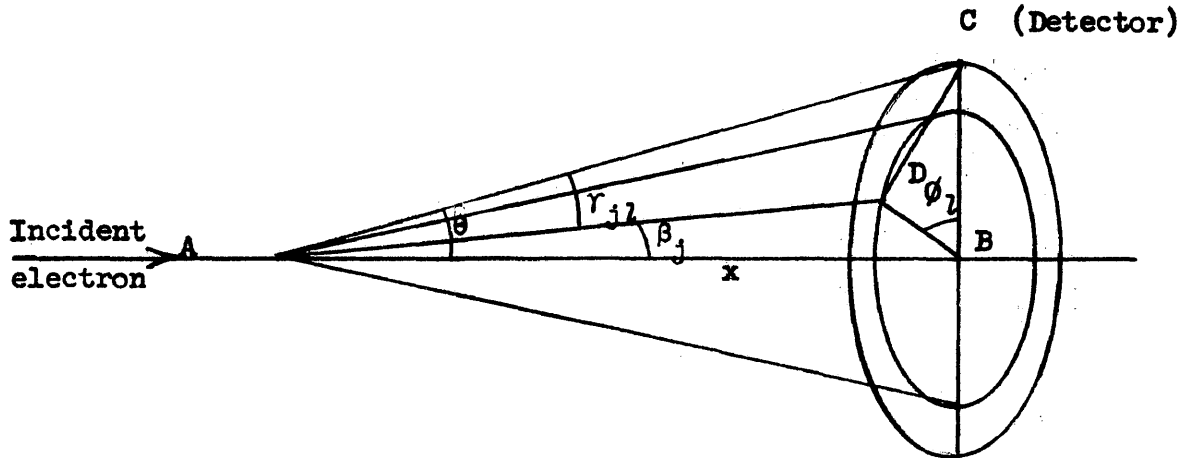With these simplifications, the thick target case can be put into the following schematic form.
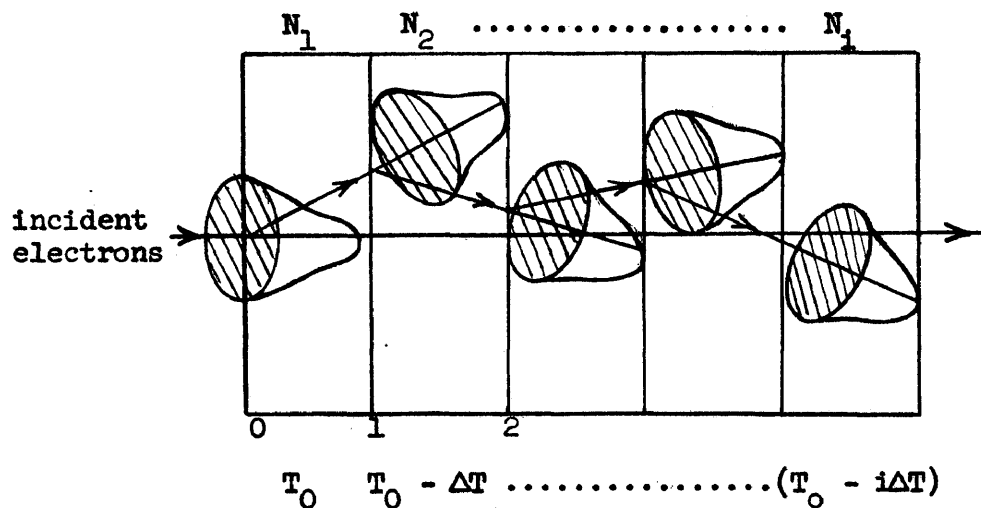
All of the scattering probability distribution energy (bells) are of the same size.

where N = number of target atoms per cm^3

ΔE = 50 kev

Ni = number of target atoms in the ith strip

The probability of scattering of an electron in any given direction is given by the differential cross section for multiple scattering in that direction. Since the electron distribution is symmetric in space about the direction of propagation of electrons in the beginning of each strip, electrons scattered through the same angle θ may be traveling in an entirely different direction with respect to the detector. This effect is allowed for as follows.

$$BD = x \tan \beta_j$$

$$AD = x \sec \beta_j$$

$$BC = x \tan \theta$$

$$AC = x \sec \theta$$

$$\cos \gamma_{jl} = \cos \theta \cos \beta_j \, (1 + \tan \theta \tan \beta_j \cos \phi_l)$$

$$= \cos \theta \cos \beta_j + \sin \theta \sin \beta_j \cos \phi_l$$

It has been assumed here that the lateral displacement of the electrons due to multiple scattering is extremely small compared to the distance of the detector from the target. Thus multiple scattering effectively changes only the direction of incidence of the electron involved in radiative collisions.

If one follows the progress of a large number of electrons through all the strips and keeps track of their directions in successive strips, one can get the overall $\frac{d^2\sigma}{dk d\theta}$.

$$\frac{d^2\sigma}{dk d\theta} = \sum_l \sum_j \sum_i N_i \left[\frac{d^2\sigma}{d\beta d\phi}(T_i, \beta_j, \phi_l)\right]_{multiple,S} \left[\frac{d^2\sigma}{dk d\gamma}(T_i, k, \gamma_{jl})\right]_{B.H.} \left[e^{-\frac{\mu(k)x}{2\cos\theta}}\right]$$

N_i = number of atoms in the ith strip

T_i = electron energy in the ith strip

β_j = semiangle of the cone

ϕ_l = azimuthal angle

γ_{jl} = angle between incident electron and emitted photon

k = energy of photon

$\mu(k)$ = attenuation coefficient in silicon for photons of energy k. It has units of cm^{-1}

θ = angle between the incident electron beam and the detector

$\frac{d^2\sigma}{d\beta d\phi}$ = multiple scattering cross section calculated from Goudsmit-Saunderson theory

$\frac{d^2\sigma}{dk d\gamma}$ = relative collision cross section as given by Bethe-Heitler theory

x = range of incident electrons in the target (target thickness in units of cm)

CHAPTER V

COMPARISON OF THEORY AND EXPERIMENTAL RESULTS

1. Figures 2, 3, 4, and 5 are typical of the observed brems-strahlung spectra. The sudden decrease in intensity after about 100 kev can be attributed to the absorption of the low energy bremsstrahlung in the target and target chamber walls.

The background is negligible in comparison with the target spectrum, and it can therefore be concluded that an assumption made during experiment was justified. This assumption was that the background bremsstrahlung created by scattered electrons of energy less than 1.05 Mev or 1.25 Mev can be approximated by bremsstrahlung from electrons of 1.05 Mev or 1.25 Mev for purposes of background corrections.

2. Figures 8, 9, 10, and 11, which compare the corrected experimental spectra with theoretical spectra (ref. 2), are not in exact agreement. There are several reasons for this discrepancy.

(a) In the theoretical calculations the electron-electron bremsstrahlung was omitted. This is expected to be $\frac{1}{Z}$ of the nuclear bremsstrahlung. Inclusion of this effect is expected to improve the agreement between theory and experiment in the lower energy region though it has no effect at the higher energy region. (Ref. 7.)

(b) The backscattering of the electrons was also omitted in the theoretical approach. The consideration of backscattering would lower the cross section for the higher energy photons most and would thus bring the two curves into better agreement.

(c) Secondary electron bremsstrahlung was also omitted in the theoretical approach. The bremsstrahlung from secondary electrons created by the primary electrons and their bremsstrahlung would make the theoretical cross section higher, particulary in the low energy region, and would thus bring the curves closer together.

(d) The angular distribution and the energy distribution for the scattering of electrons which were used in the theoretical approach were compared with experimental data (ref. 3) on electron scattering and the comparison showed that the actual distributions are broader than those used in the theory. This would bring the theoretical curve closer to the experimental one.

(e) The theoretical approach did not take into account the screening effects of the atomic electrons on the nucleus. Thus, the theory overestimates the radiative collision cross section.

(f) Error in the experimental curve could have been introduced by the fact that the NaI (Tl) detector efficiencies used in the calculations were theoretical.

3. The shape of figures 12 and 13, which show the angular distribution of three sections of the X-ray spectrum, is in agreement with previous reports (ref. 2). The curve for the highest

energy photons is steep indicating the relative number of photons
in the high frequency region increases sharply as the emission
angle becomes smaller. The lower energy sections show a broader
distribution as is expected.

4. Figures 14 and 15, which show the angular distribution
of the total intensity, indicate that the angular dependence of
the intensity is slightly dependent on the incident electron energy.
The higher the incident electron energy the steeper the curve for
angular distribution.

5. The efficiencies of the radiative collisions given in
table III are reasonably close to the theoretical values. An
empirical expression of the type

$$\epsilon \simeq 0.0004 ZE$$

for electron energies in the range 1-3 Mev has been suggested by
Buechner, et al. (ref. 5). However, the efficiences calculated
in this paper come closer to fitting the equation

$$\epsilon \simeq 0.0004 ZE^2$$

CHAPTER VI

CONCLUSIONS

1. The experimental results and the theoretical model are in reasonable, although not exact, agreement.

2. The angular distribution of the radiated flux is strongly dependent on the energy of the radiated photons. It is only slightly dependent on the energy of the incident electron (ref. 8).

3. An empirical relation giving the expected efficiency as a function of the incident electron energy has been derived and the thick target bremsstrahlung efficiency is proportional to the square of the electron energy.

REFERENCES

1. W. H. Koch and J. W. Motz, Rev. Mod. Phys. 31, 920 (1959).

2. J. J. Singh, Bull. Am. Phys. Soc. 9, 50 (1964); Bull. Am.
   Phys. Soc. 9, 297 (1964).

3. J. J. Singh, Bull. Am. Phys. Soc. 10, 68 (1965).

4. L. Katz and A. S. Penfold, Rev. Mod. Phys. 24, 28 (1952).

5. W. W. Buechner, R. J. Van de Graaff, E. A. Burrill, and
   A. Sperduto, Phys. Rev. 74, 1348 (1948).

6. R. E. Evans, The Atomic Nucleus, (McGraw-Hill Book Company,
   New York, 1955).

7. J. W. Motz, Phys. Rev. 100, 1560 (1955).

8. W. Miller, J. W. Motz, and C. Ciallella, Phys. Rev. 96, 1344 (1954).

9. G. W. Grodstein, National Bureau of Standards Circular 583 (1957).

10. R. T. McGinnies, National Bureau of Standards Supplement to
    Circular 583 (1959).

TABLE I

ANGULAR DISTRIBUTION OF THE X-RAYS PRODUCED WHEN 1.05 MEV AND 1.25 MEV

ELECTRONS BOMBARDED THICK SILICON TARGETS

Electron energy	Energy interval (keV)	Angular distribution expression $I(\theta)$
1.25	1250-850	$P_o - (2.58 \pm 0.10)P_1 + (1.98 \pm 0.08)P_2 - (1.26 \pm 0.03)P_3$
	850-450	$P_o - (2.63 \pm 0.10)P_1 + (2.04 \pm 0.08)P_2 - (0.90 \pm 0.03)P_3$
	450-100	$P_o - (2.65 \pm 0.18)P_1 + (2.09 \pm 0.01)P_2 - (1.34 \pm 0.01)P_3$
1.05	1050-750	$P_o - (2.64 \pm 0.12)P_1 + (2.02 \pm 0.08)P_2 - (1.30 \pm 0.04)P_3$
	750-450	$P_o - (2.68 \pm 0.23)P_1 + (2.13 \pm 0.19)P_2 - (1.30 \pm 0.09)P_3$
	450-150	$P_o - (2.90 \pm 0.23)P_1 + (2.26 \pm 0.12)P_2 - (1.39 \pm 0.08)P_3$

$P_i = P_i(\cos \theta)$

$i = 0,1,2,3,\ldots$

TABLE II

ANGULAR DISTRIBUTION OF TOTAL RADIATED ENERGY FROM THICK SILICON TARGETS

BOMBARDED WITH 1.05 AND 1.25 MEV ELECTRONS

Electron energy (meV)	Angular distribution expression $I(\theta)$
1.25	$P_o - (2.63 \pm 0.03)P_1 + (2.07 \pm 0.02)P_2 - (1.33 \pm 0.01)P_3$
1.05	$P_o - (2.86 \pm 0.25)P_1 + (2.21 \pm 0.19)P_2 - (1.37 \pm 0.09)P_3$

$P_i = P_i(\cos \theta)$

$i = 0,1,2,3,....$

TABLE III

EFFICIENCY OF RADIATIVE COLLISIONS IN SILICON

Electron energy	$\dfrac{\text{Total radiated energy}}{\text{Incidental energy}}$ (Percent)	Theoretical efficiency (ref. 2)
1.25	0.81 ± 0.08	0.89
1.05	0.56 ± 0.06	0.71
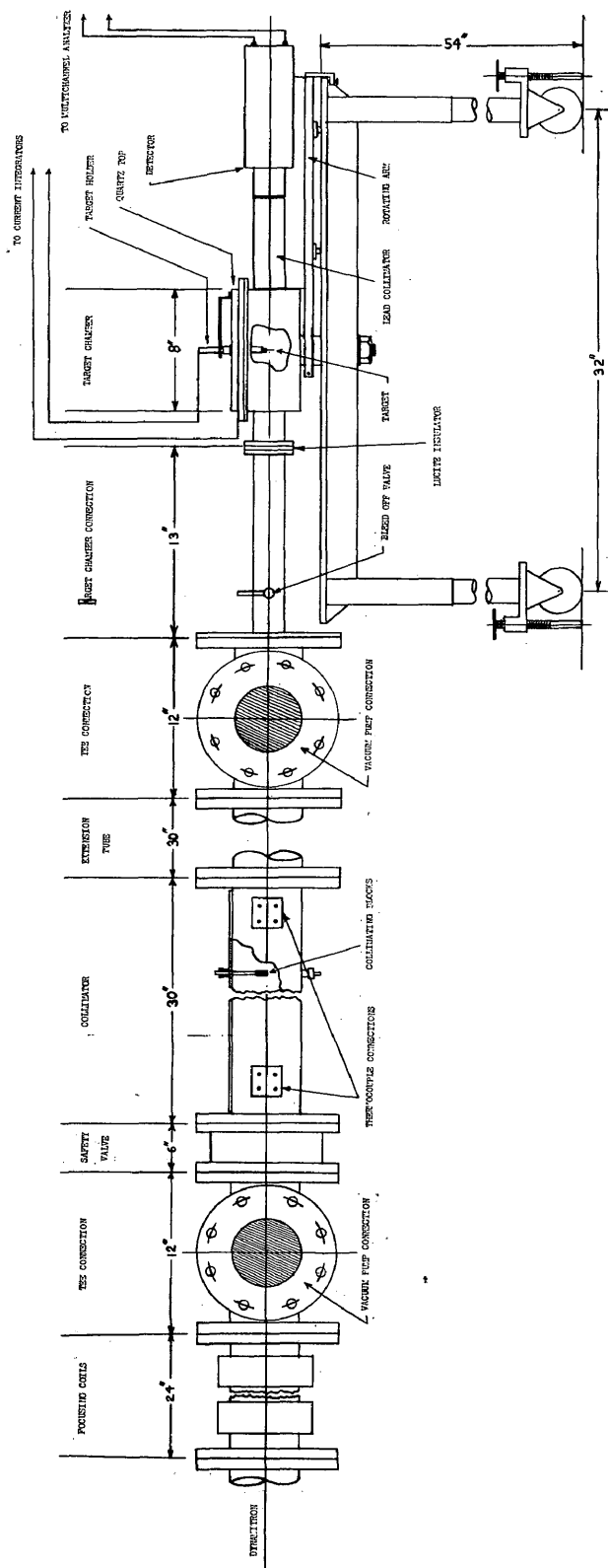
Figure 1.— Beam tube assembly.
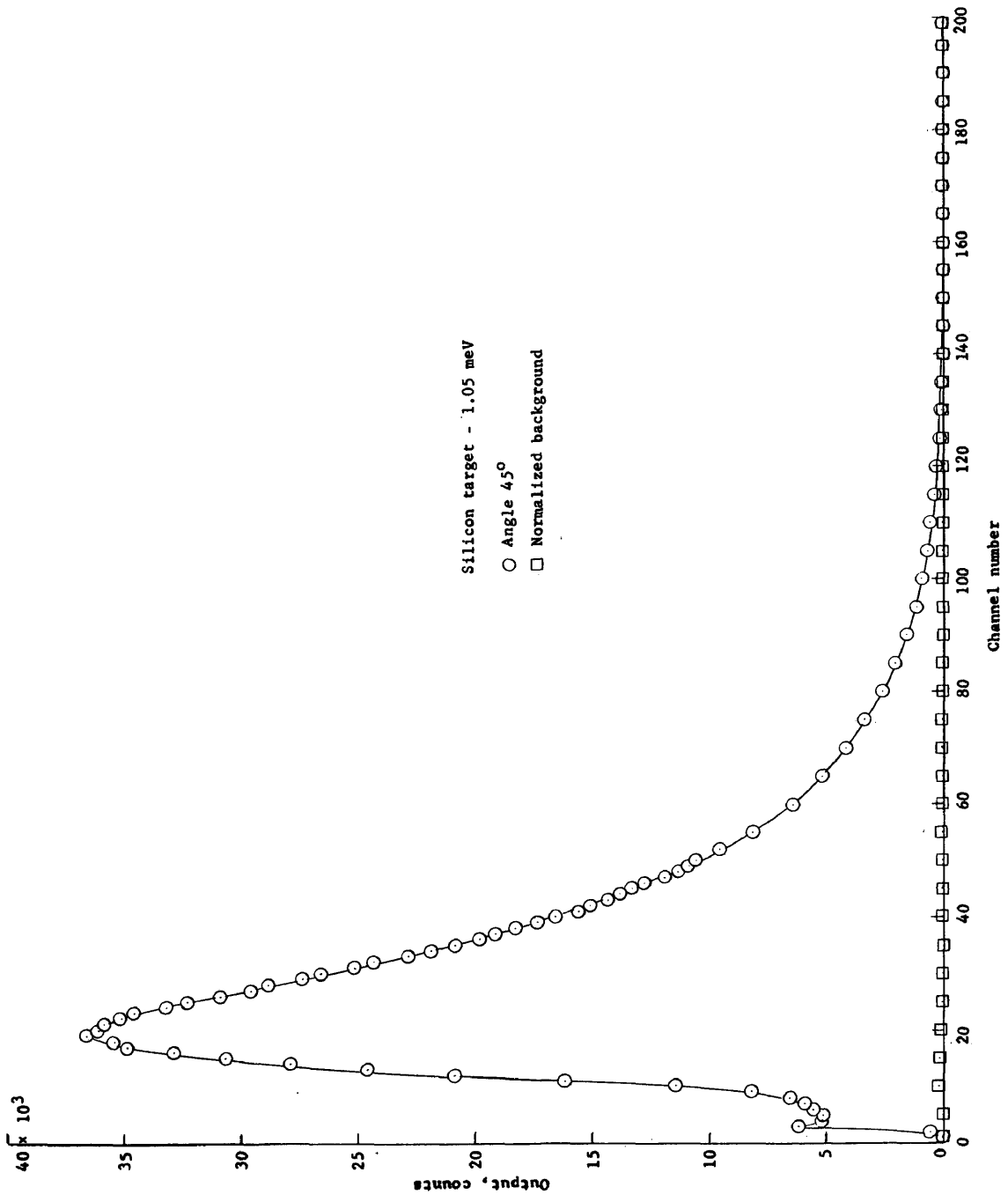
Figure 2.— The observed spectrum at 45° when 1.05 meV electrons bombarded the thick silicon target. The normalized background is also shown.
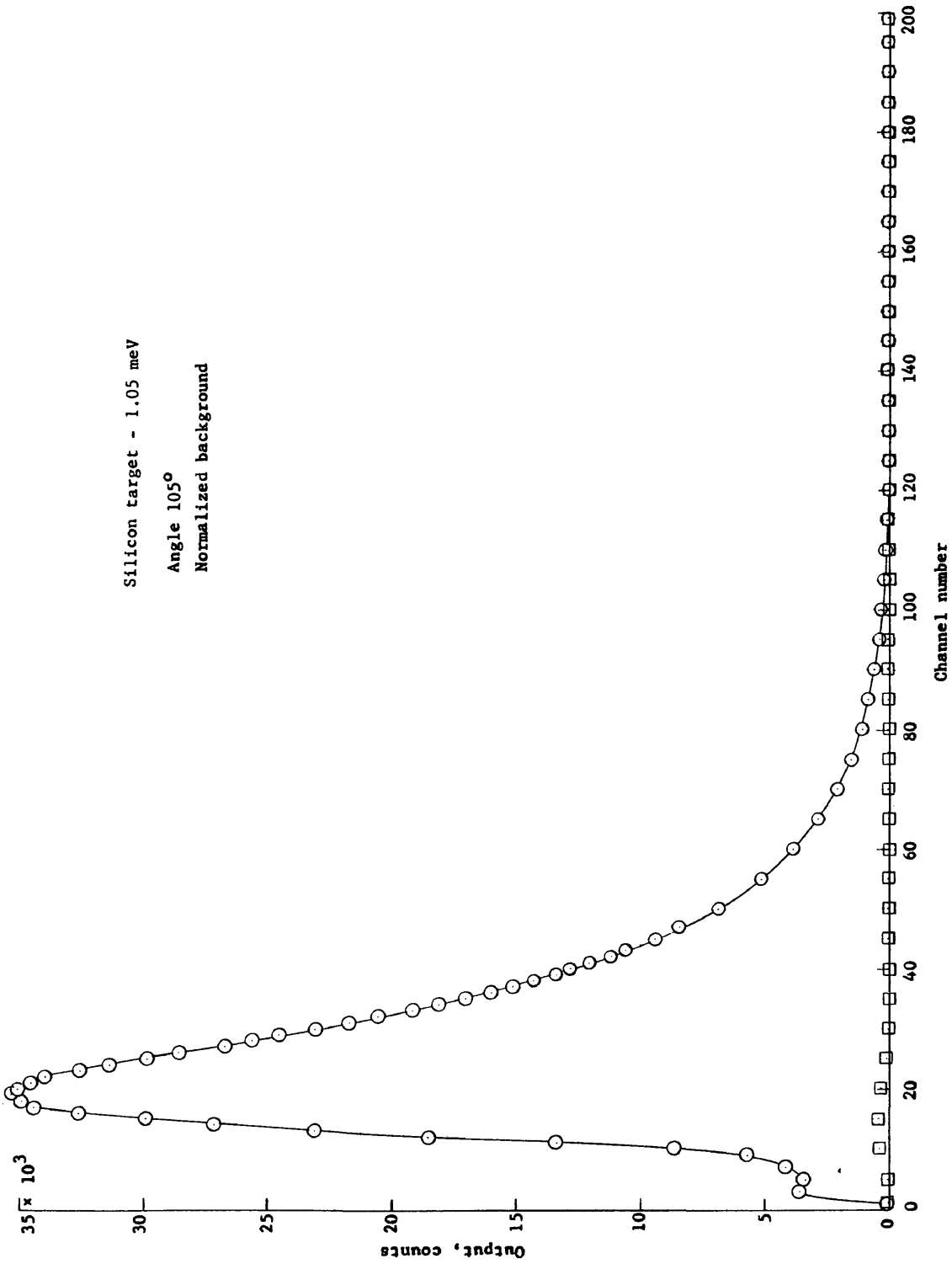
Figure 3.— The observed spectrum at 105° when 1.05 meV electrons bombarded the thick silicon target. The normalized background is also shown.
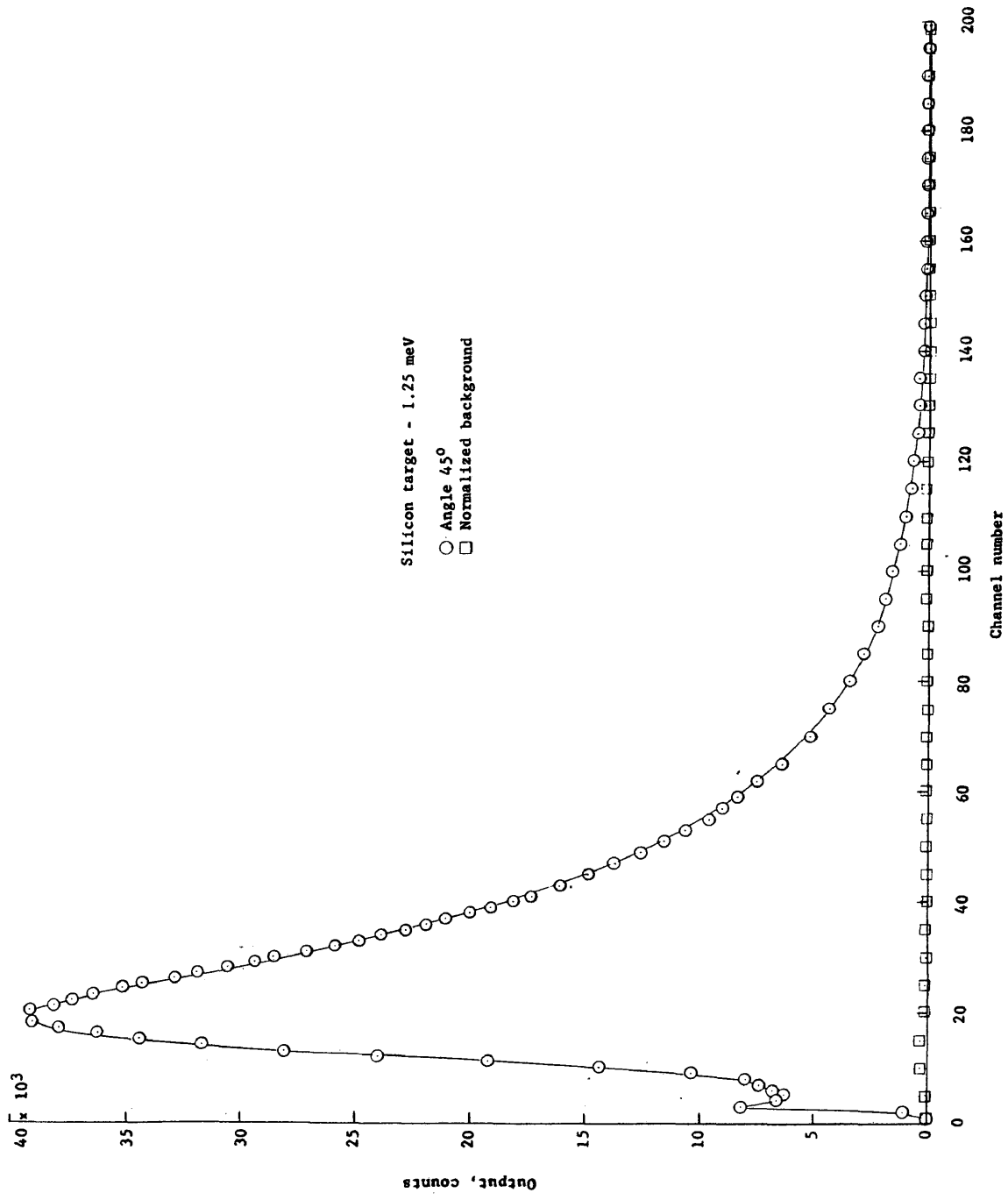
Figure 4.— The observed spectrum at 45° when 1.25 meV electrons bombarded the thick silicon target. The normalized background is also shown.
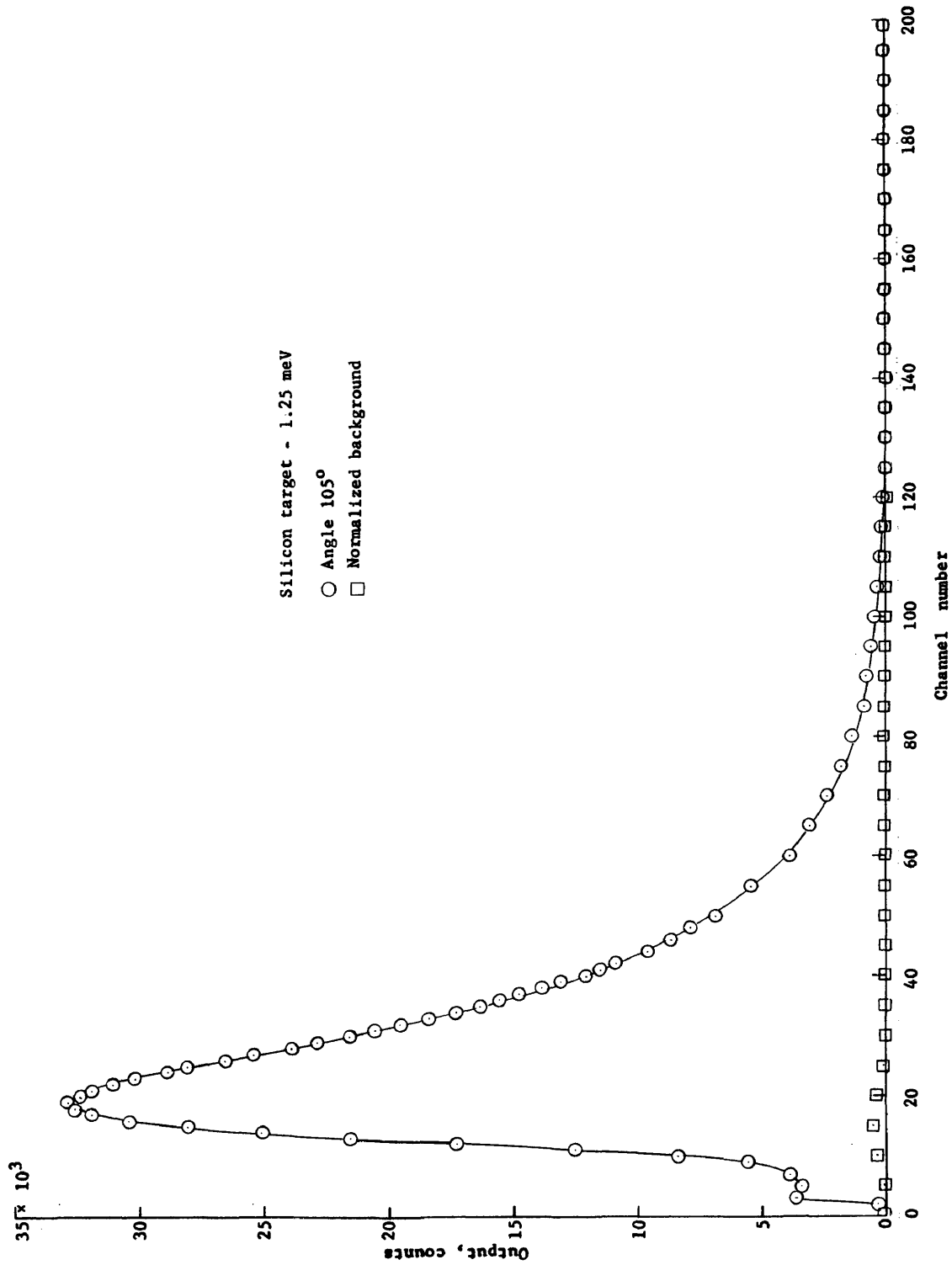
Figure 5.— The observed spectrum at 105° when 1.25 meV electrons bombarded the thick silicon target. The normalized background is also shown.
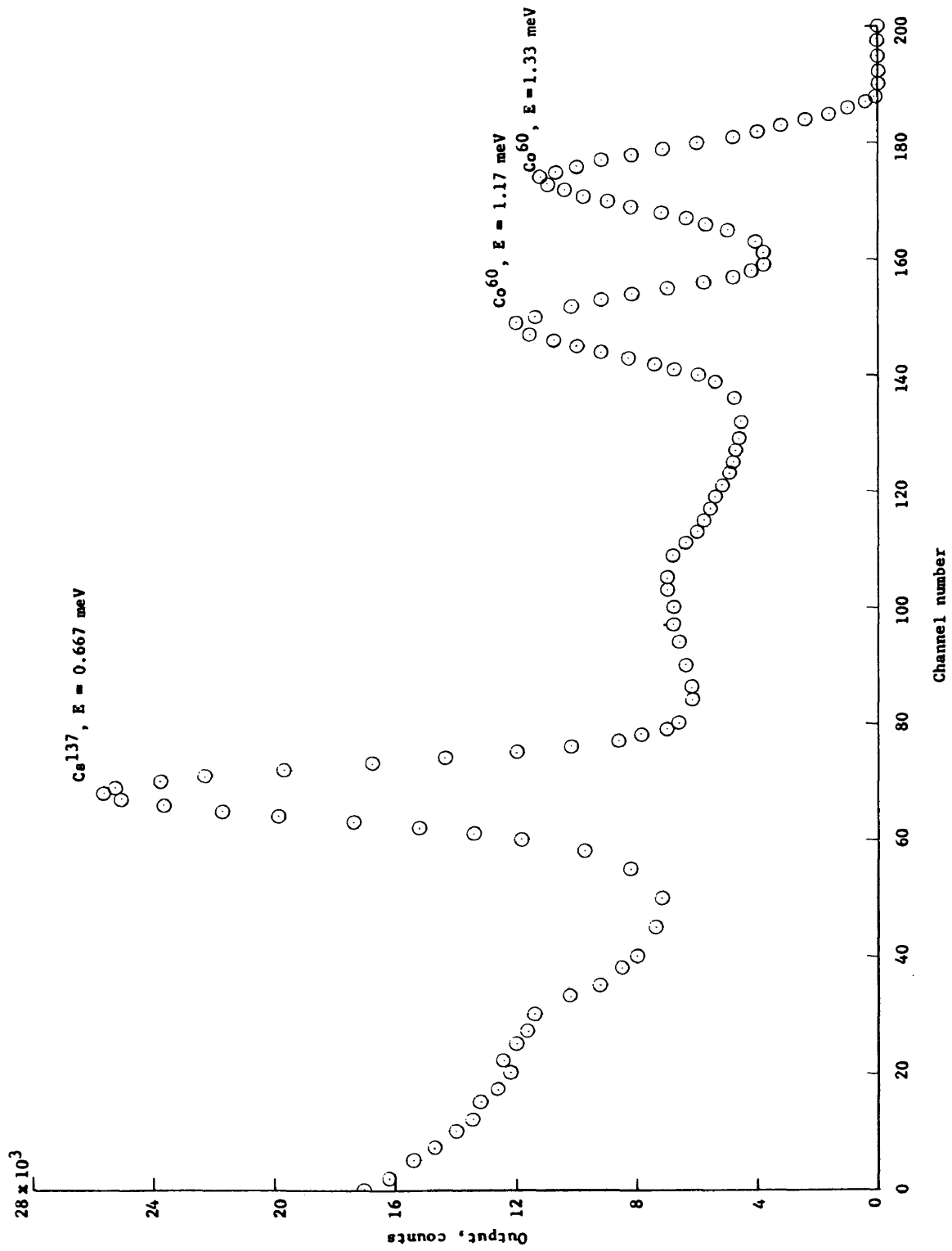
Figure 6.— Calibration of the movable detector.
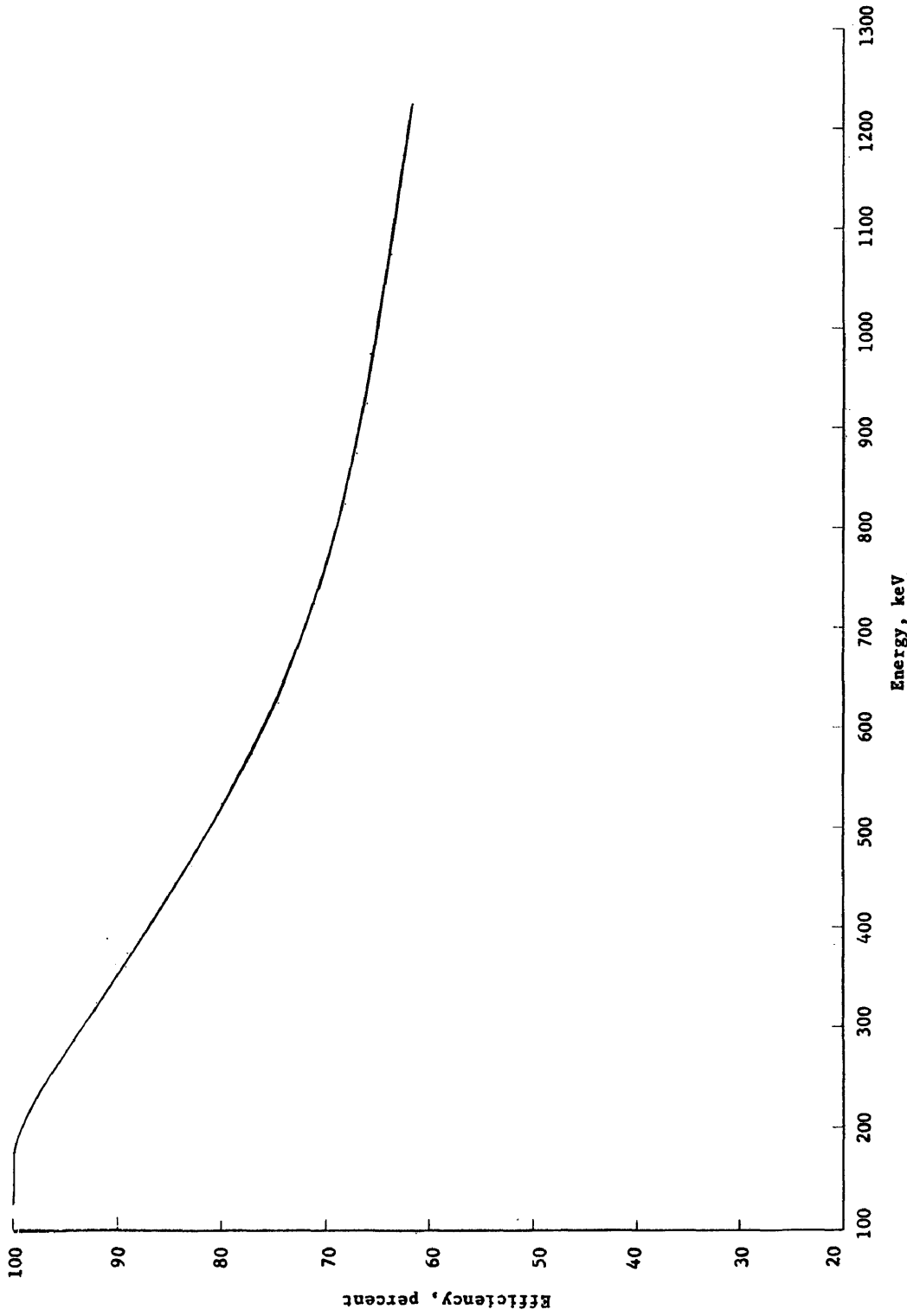
Figure 7.— Sodium iodide (NaI) crystal efficiency.

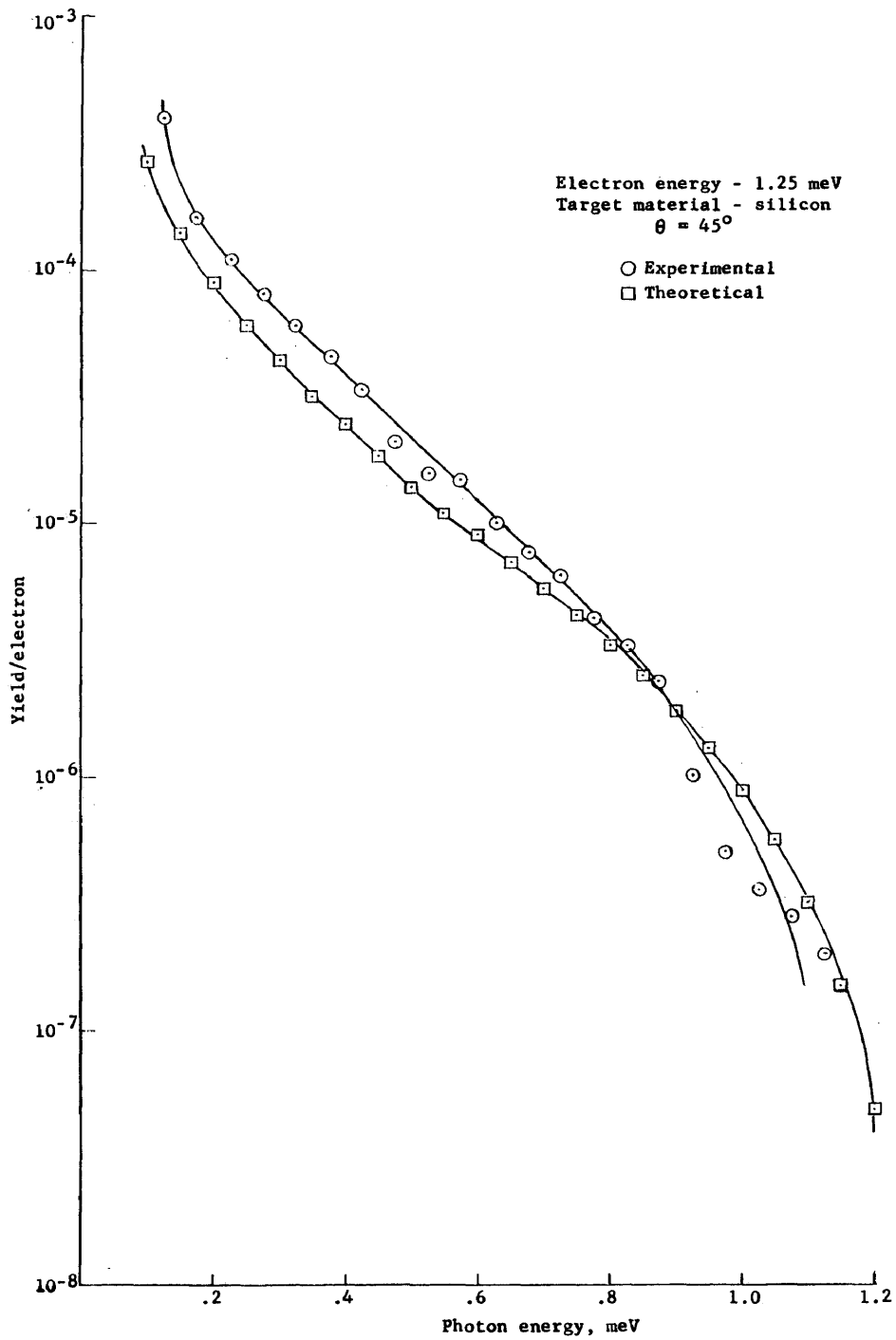The attenuation coefficients used in the theoretical efficiency calculations are given in references 9 and 10.
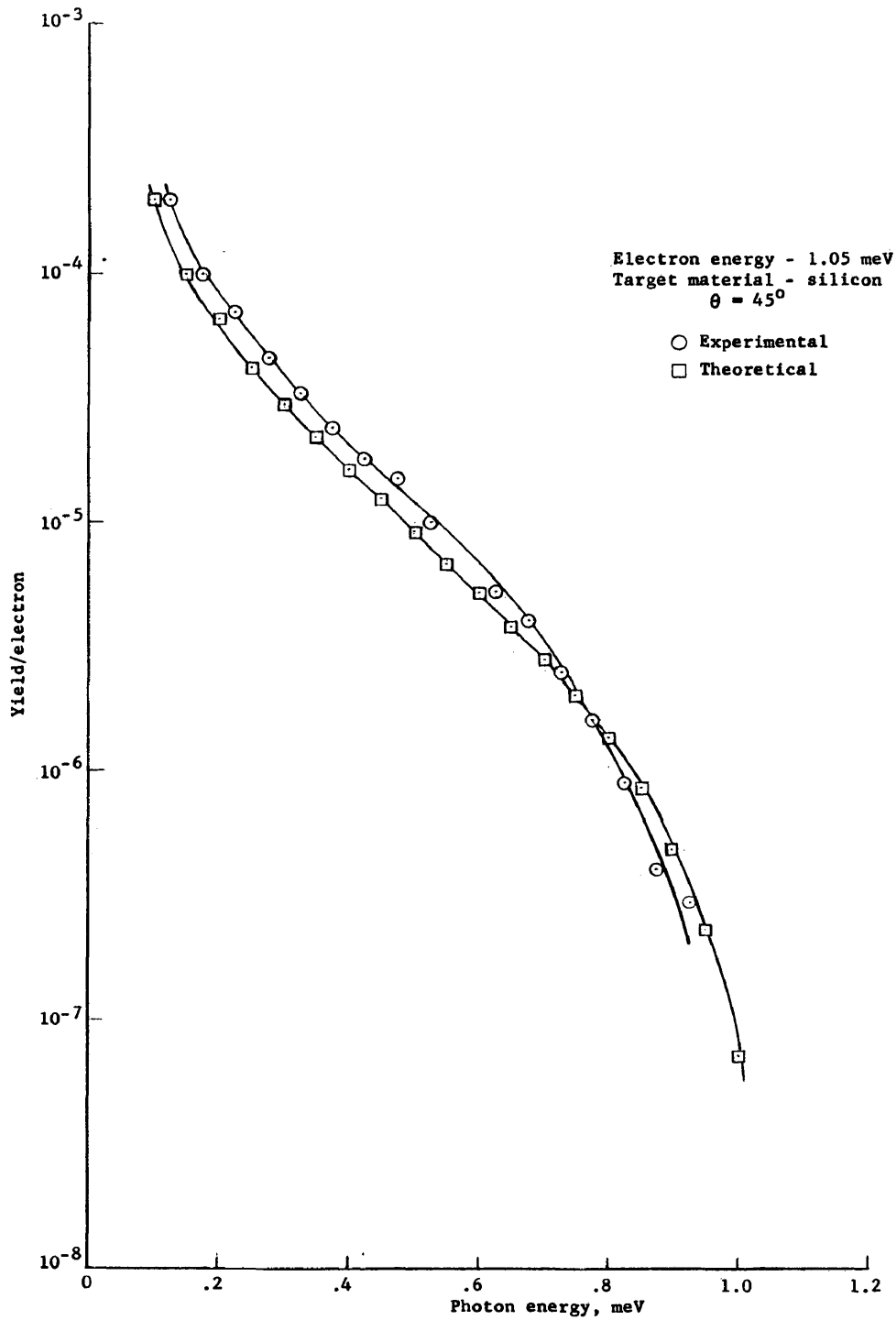
Figure 8.— Comparison of the corrected experimental spectrum
and the theoretical spectrum at 1.05 meV.
The detector is located at 45°.
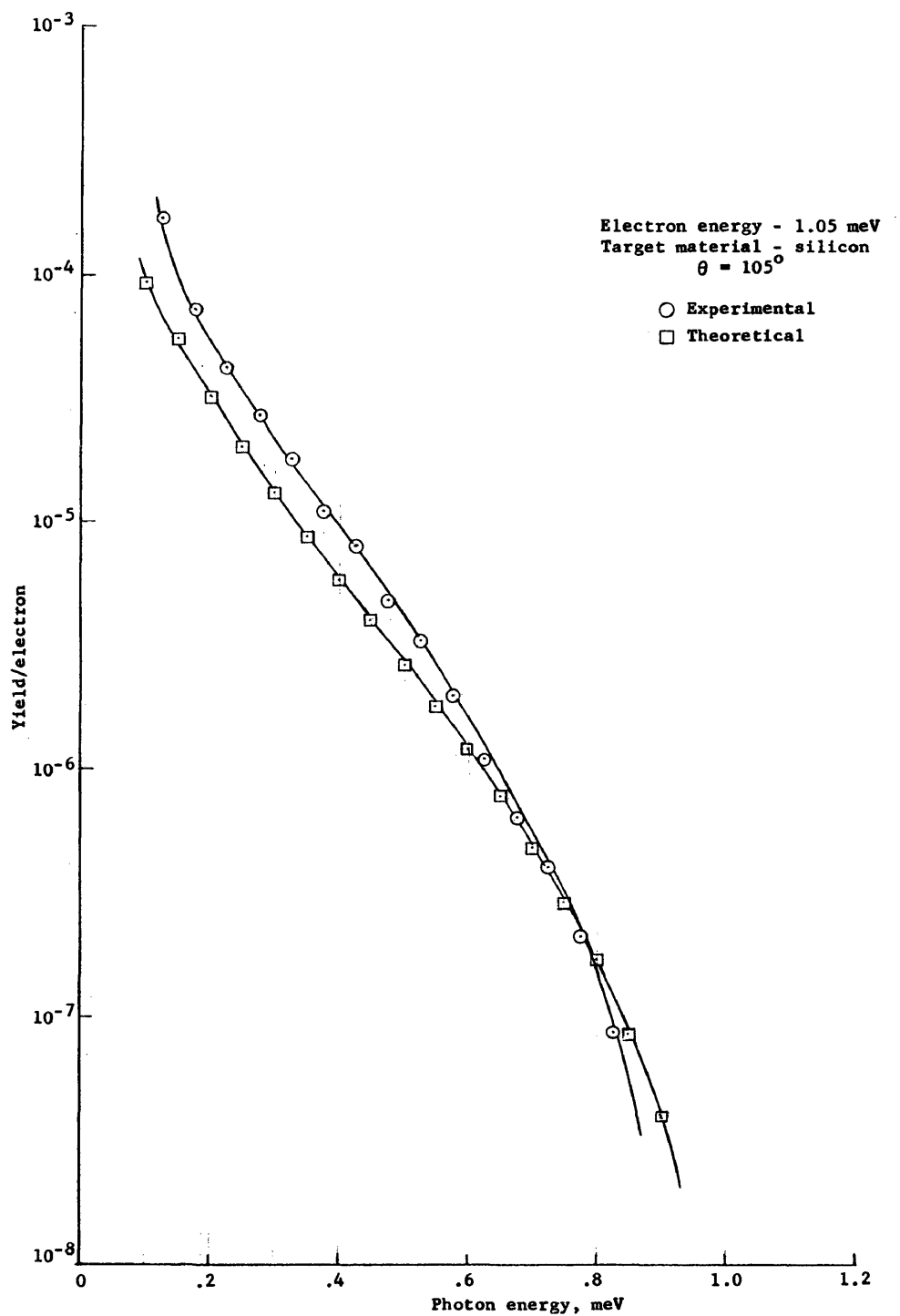
Figure 9.— Comparison of the corrected experimental spectrum
and the theoretical spectrum at 1.05 meV.

The detector is located at 105°.

10^{-3}

Electron energy - 1.25 meV
Target material - silicon
$\theta = 45^\circ$

O Experimental
□ Theoretical

10^{-4}

10^{-5}

Yield/electron

10^{-6}

10^{-7}

10^{-8}

.2   .4   .6   .8   1.0   1.2

Photon energy, meV

Figure 10.— Comparison of the corrected experimental spectrum
and the theoretical spectrum at 1.25 meV.

The detector is located at 45°.
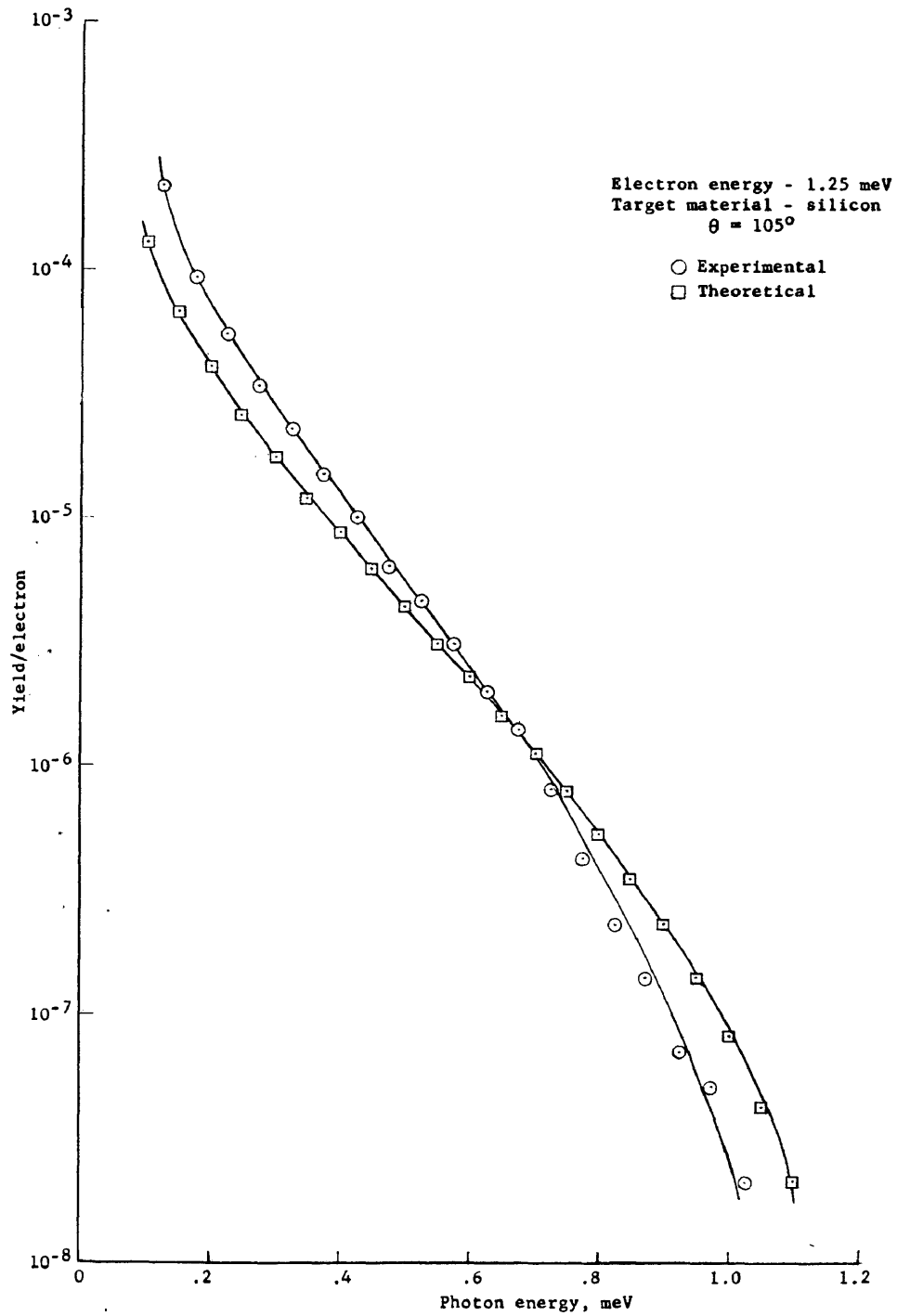
Figure 11.— Comparison of the corrected experimental spectrum
and the theoretical spectrum at 1.25 meV.
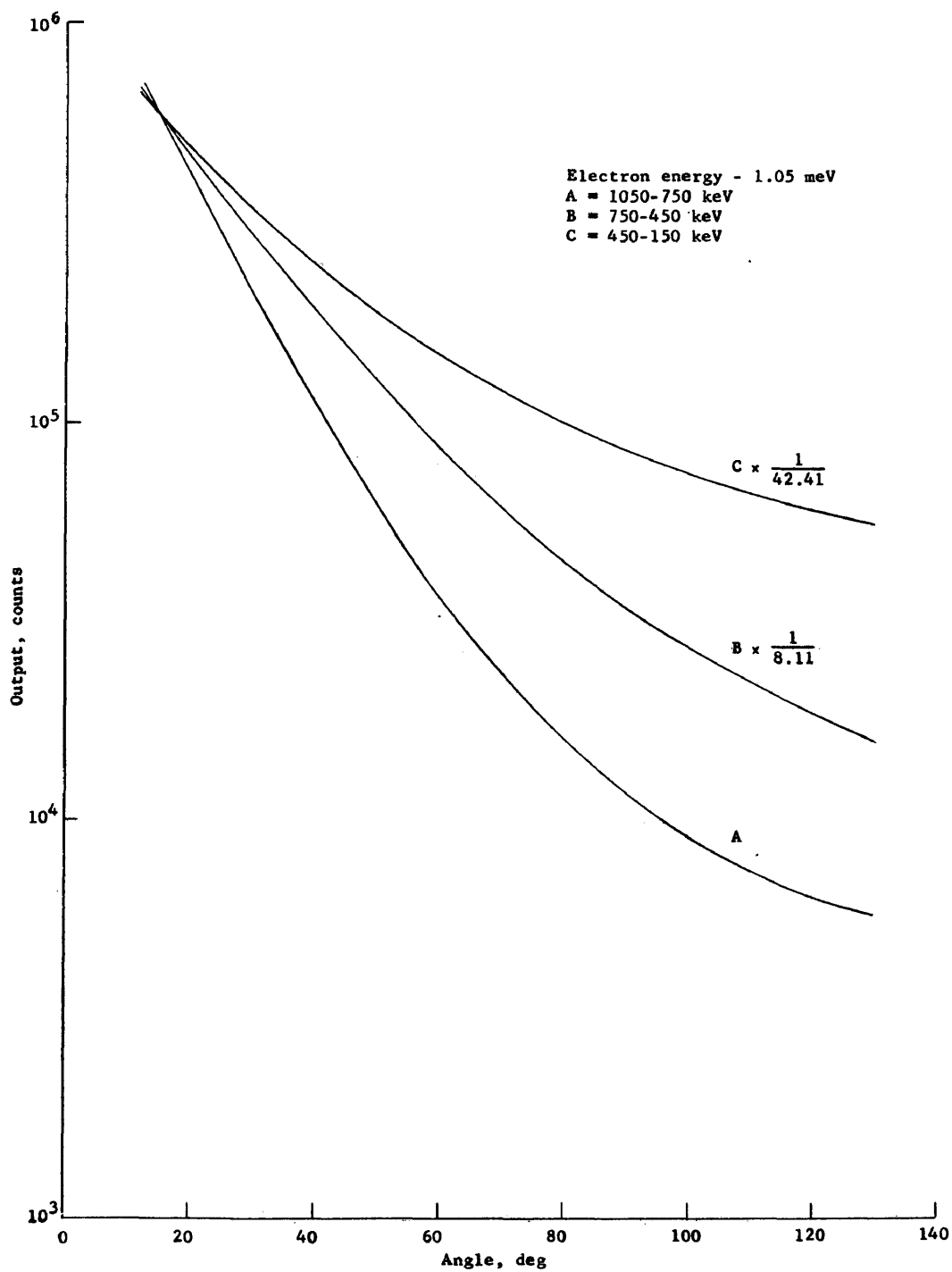The detector is located at 105°.

Figure 12.— Angular distribution of three sections of the x-ray spectrum
produced when a thick silicon target was bombarded
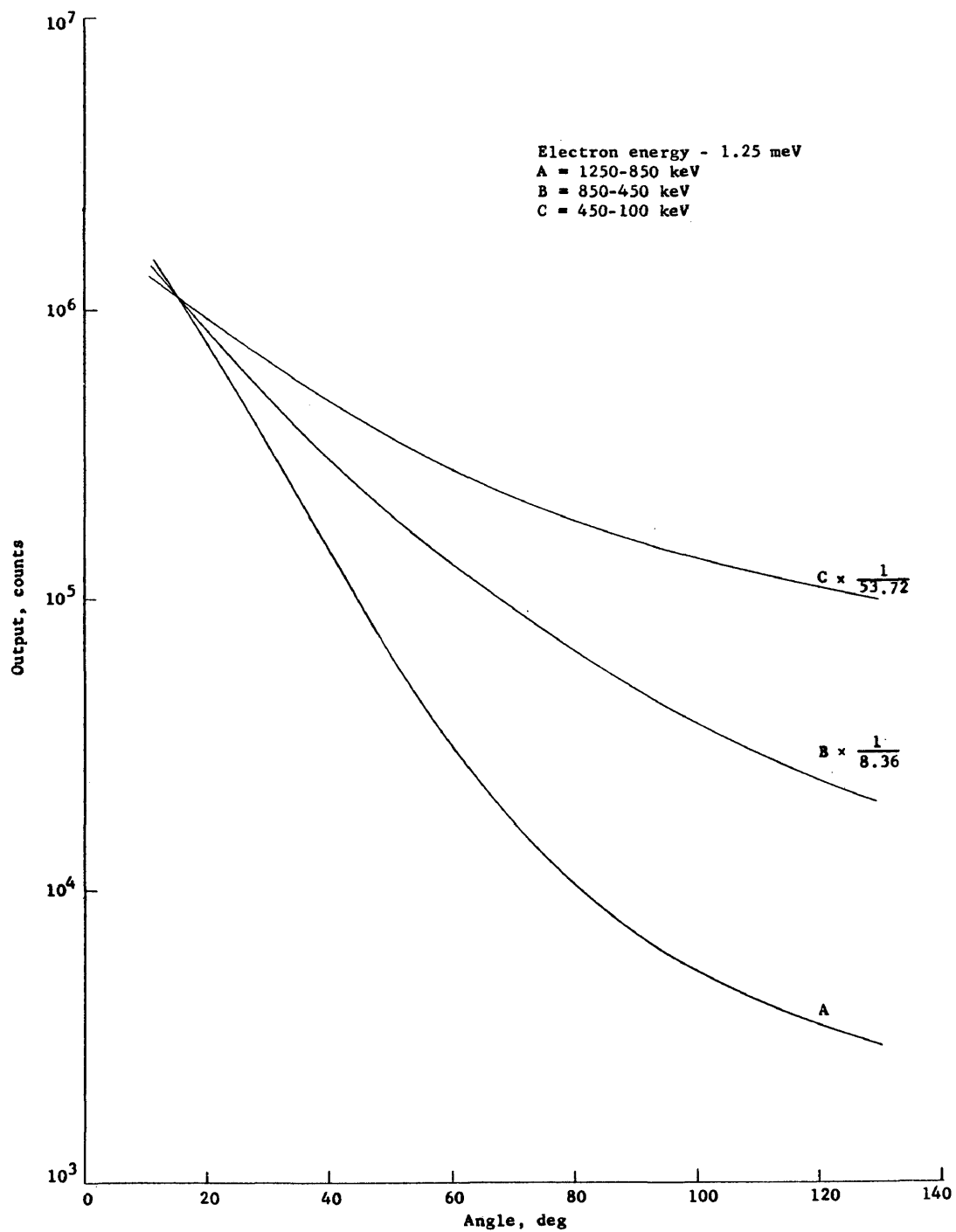with 1.05 meV electrons.

Figure 13.— Angular distribution of three sections of the x-ray spectrum
produced when a thick silicon target was bombarded
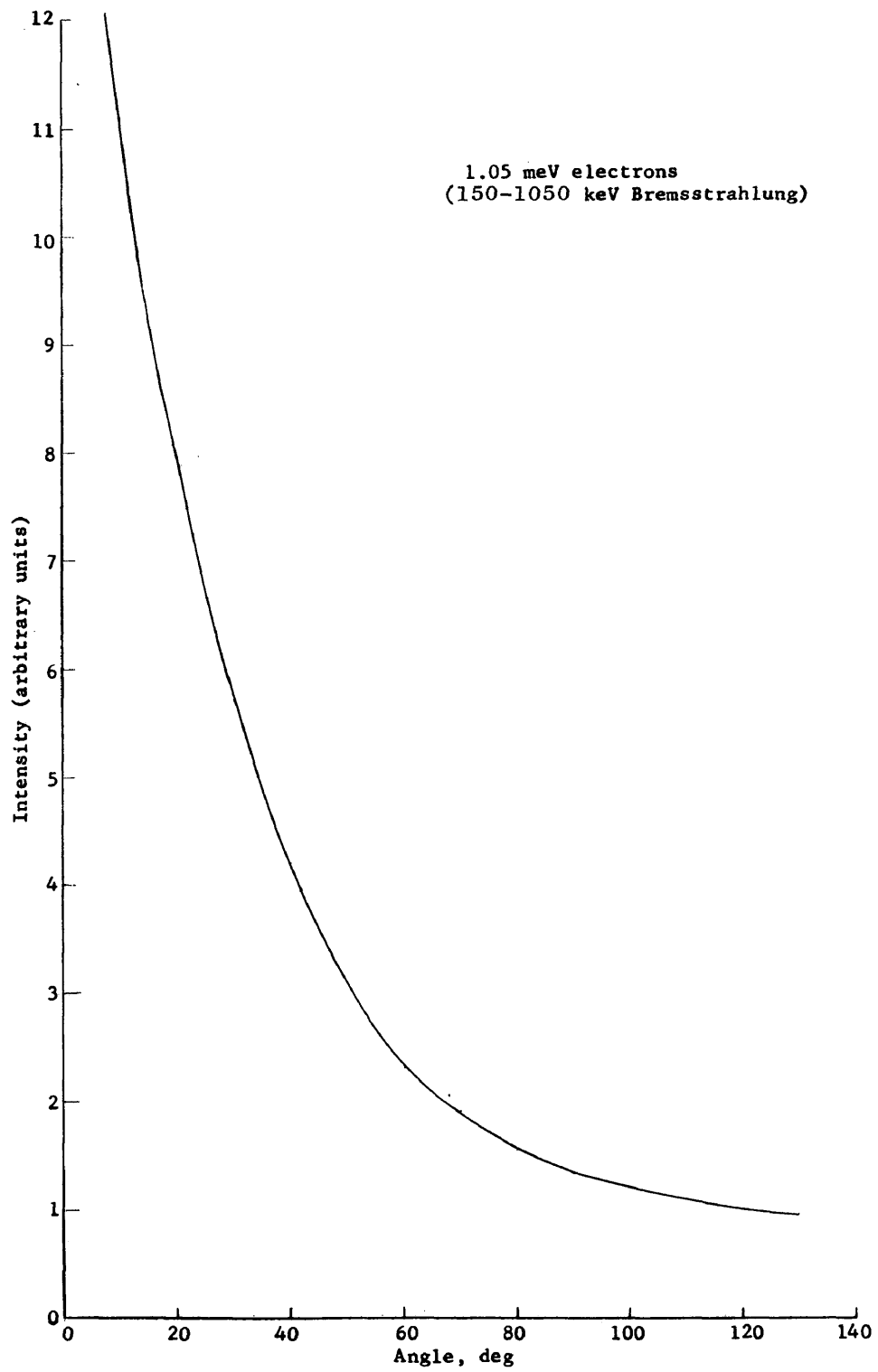with 1.25 meV electrons.

1.05 meV electrons
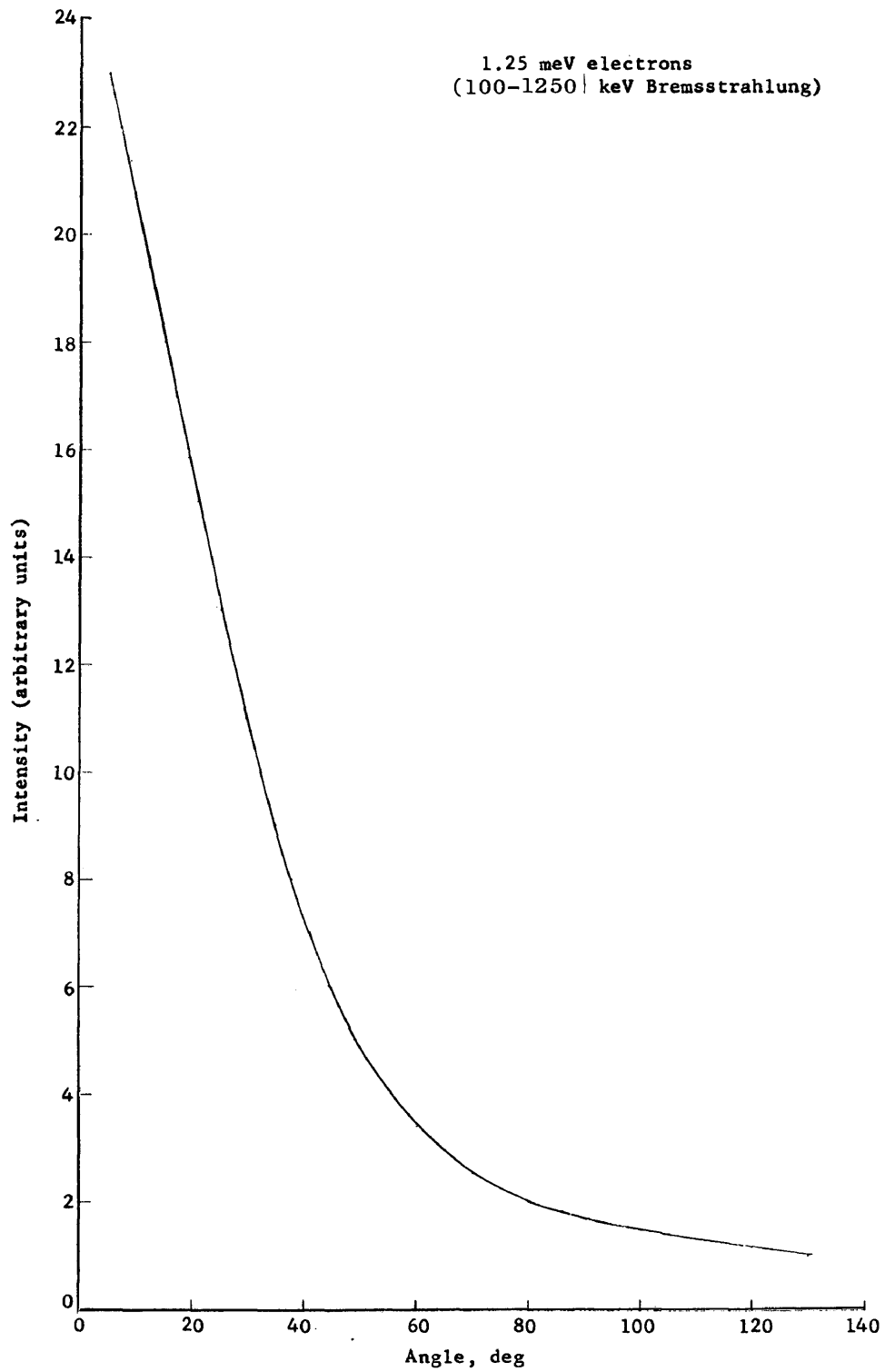(150-1050 keV Bremsstrahlung)

Figure 14.— Angular distribution of total intensity.

Figure 15.— Angular distribution of total intensity.